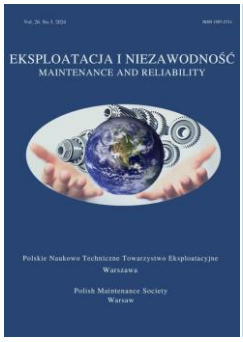

Eksploatacja i Niezawodnosc – Maintenance and Reliability
Volume 26 (2024), Issue 3
journal homepage: http://www.ein.org.pl

Article citation info:
S.S.K. Singh, L. Abdullah, S. Abdullah, A.H Azman, , A.K. Ariffin, Strain-based running-reliability characterisation in time-domain for risk monitoring under various load conditions, Eksploatacja i Niezawodnosc – Maintenance and Reliability 2024: 26(3) http://doi.org/10.17531/ein/186825

Strain-based running-reliability characterisation in time-domain for risk monitoring under various load conditions

Indexed by:
Web of Science Group

S.S.K. Singh[a,*], L. Abdullah[a], S. Abdullah[a], A.H. Azman[a], A.K. Ariffin[a]

[a] Department of Mechanical and Manufacturing Engineering, Faculty of Engineering and Built Environment, Universiti Kebangsaan Malaysia,

Highlights

- Running reliability is proposed for assessing extreme value distribution in time domain.
- Cycle sequence load is proposed for fatigue life prediction.
- Fatigue reliability is numerically assessed from experimental data.
- Running reliability has the capability of failure monitoring.

Abstract

This aim of this paper is to characterise the strain-based fatigue life data in time-domain using the newly modelled running-reliability technique that considers the load sequence effect. Current established conventional strain life models do not consider dependence for fatigue life of low or high amplitudes, on which with occur first in the load history. Finite element analysis is carried out to ensure the strain signals are captured at the most critical region during road test at various conditions. Fatigue life of 2.74×10^4 to 6.07×10^5 cycle/block with mean cycle to failure of 4.32×10^6 to 7.00×10^6 cycle/block is predicted based on the cycle sequence effect using cycle-counting method. The newly modelled running-reliability technique is formulated to extract the features of high amplitude excitation obtained from the strain signals for characterising the fatigue reliability features under load sequence effect. Hence, the reliability-hazard relationship for fatigue reliability characterisation of strain-based approach in time-domain using running-reliability technique.

Keywords
strain loads, mean cycle to failure, time-domain, running-reliability, risk monitoring.

1. Introduction

In the automotive industry, fatigue reliability assessment is important as it is related to fatigue life data assessment under random load condition for failure prediction of components or structures [1]. For example, the leaf spring is an important component that experiences random loads in terms of compression-tension based on its operating conditions [2]. The laminated leaf spring is placed between the vehicle axle and wheel where one of the eyes of the leaf spring is a fixed end while the other eye is a movable end. The effects of bending acting on the leaf spring is produced by absorbing a vibration or shock when travelling a pothole or bump on road profiles. This effect contributes to a comfortable and safe ride [3]. The study of finite element analysis is needed in monitoring purposes for failure occurred on a component or structure. Recent study involved identifying the stiffness condition on a structure, investigating a polygonal finite element on a steady fluid problem, and predicting a hardness for low carbon steel of a component [4-6]. In addition to that, analysis of finite

(*) Corresponding author.
E-mail addresses: S.S.K.Singh (ORCID: 0000-0002-5549-9019) salvinder@ukm.edu.my, L. Abdullah (ORCID: -0000-0002-2130-7103) p94883@siswa.ukm.edu.my, S.Abdullah (ORCID: 0000-0003-0345-5628) shahrum@ukm.edu.my, A. H. Azman (ORCID: 0000-0001-5349-7768) hadi.azman@ukm.edu.my, A. K. Ariffin (ORCID: 0000-0001-5098-5088) kamal3@ukm.edu.my

element-based is implemented in predicting a crack propagation of quasi-brittle material and optimising a buckling of porous microplates material [7, 8].

The fatigue life data characteristics is an important technique for assessing the components or structures life when subjected to cyclic loading. The mean stress effects in every load cycle resulted a fatigue failure for the suspension system under cyclic loading especially on a coil spring [9], antiroll bar [10], shackle bracket [11], and leaf spring [12] due to cyclic flexural. The influence of mean stress is needed in predicting fatigue life by applying the traditional strain-life models, i.e. Morrow and Smith-Watson-Topper models. In addition, the strain-life models excluded the sequence of load cycle effect in assessing the fatigue life of components and structures [13]. The advantage of using the load cycle sequence effect-based model, namely effective strain damage (ESD), is to predict fatigue life in various materials associated with a variety of loading data. The ESD model is able in predicting fatigue life in a large selection of materials in numerous types of load conditions and also considers the mean stress effect [14].

Fatigue failure based on random loads has been closely related to the statistics and probabilistic approaches for identifying the properties of the strain signals [15]. In addition, fatigue damage uses the probabilistic technique for characterising low cycle fatigue using the Gumbel distribution to predict crack growth on nodular cast-irons [16, 17]. The use of various distributions such as Gaussian and Gumbel distribution was proposed by Gong [18] in order to characterise the reliability of a hull girder at different times based on corrosion growth copulas. Additionally, Long [19] identified the uncertainties of propagation through fatigue crack growth by observing a function plots of probability density and cumulative distribution associated with random loads.

Reliability assessment is a stochastic approach that uses probabilistic models for the purpose of predicted the failure which can be modelled through the extreme value distribution. Fernández-Canteli [20] monitored the probability of failure using the generalised extreme value to characterise fatigue and fracture. In addition, the extreme value distribution was proposed by [21, 22] to identify the fatigue indicator of crack growth of microstructures and model the reliability-based method to statistically define a detection of damage for beam structure in real and simulated data in the time and frequency domains [23]. Zheng et al. [24] used extreme value theory based on a multi-axial load spectrum in fatigue analysis on special vehicle component. Wang et al. [25] also Gumbel distribution to calculate fatigue damage of vehicle components, and resulting has a best fit for extreme loads.

This study aims to propose the newly modelled running-reliability technique for the assessment of fatigue reliability under time-domain based on strain-based road load conditions. The established strain-life model and cycle sequence effect model were applied to predict fatigue life data from various road load profiles on a suspension component. The strain-life model was chosen in the fatigue damage calculation due to leaf spring is having a tension and compression conditions that contributes to a fatigue life on automotive component. In addition, the reliability assessment fatigue-based that subjected to a fatigue life data was used to predict risk based on the features of high amplitude excitation. The high amplitude excitation features were extracted to model running-reliability based on the captured strain-based loads for risk monitoring that involves the effects of the cycle sequence. This newly proposed running-reliability technique is important as it defines the reliability rate of the damage segment in time domain that has the capability to be applied for risk monitoring of a fatigue failure.

2. Methodology framework for running-reliability technique

This study proposes a newly modelled running-reliability technique in time-domain using a strain-based fatigue life data in characterising a probability of failure for an automotive leaf spring. Fig. 1 illustrates the process flow for fatigue reliability characteristics in modelling a running-reliability technique under random strain loads. The framework of fatigue reliability assessment methodological for running-reliability technique under strain-based loads is illustrated in Fig. 2. The framework is divided into three phases:

(1) Phase 1: Finite element analysis and data collection based on captured strain loads.

(2) Phase 2: Fatigue life characterisation based on time-domain for various road load conditions.

(3) Phase 3: Running-reliability for fatigue failure risk monitoring under random strain loads.

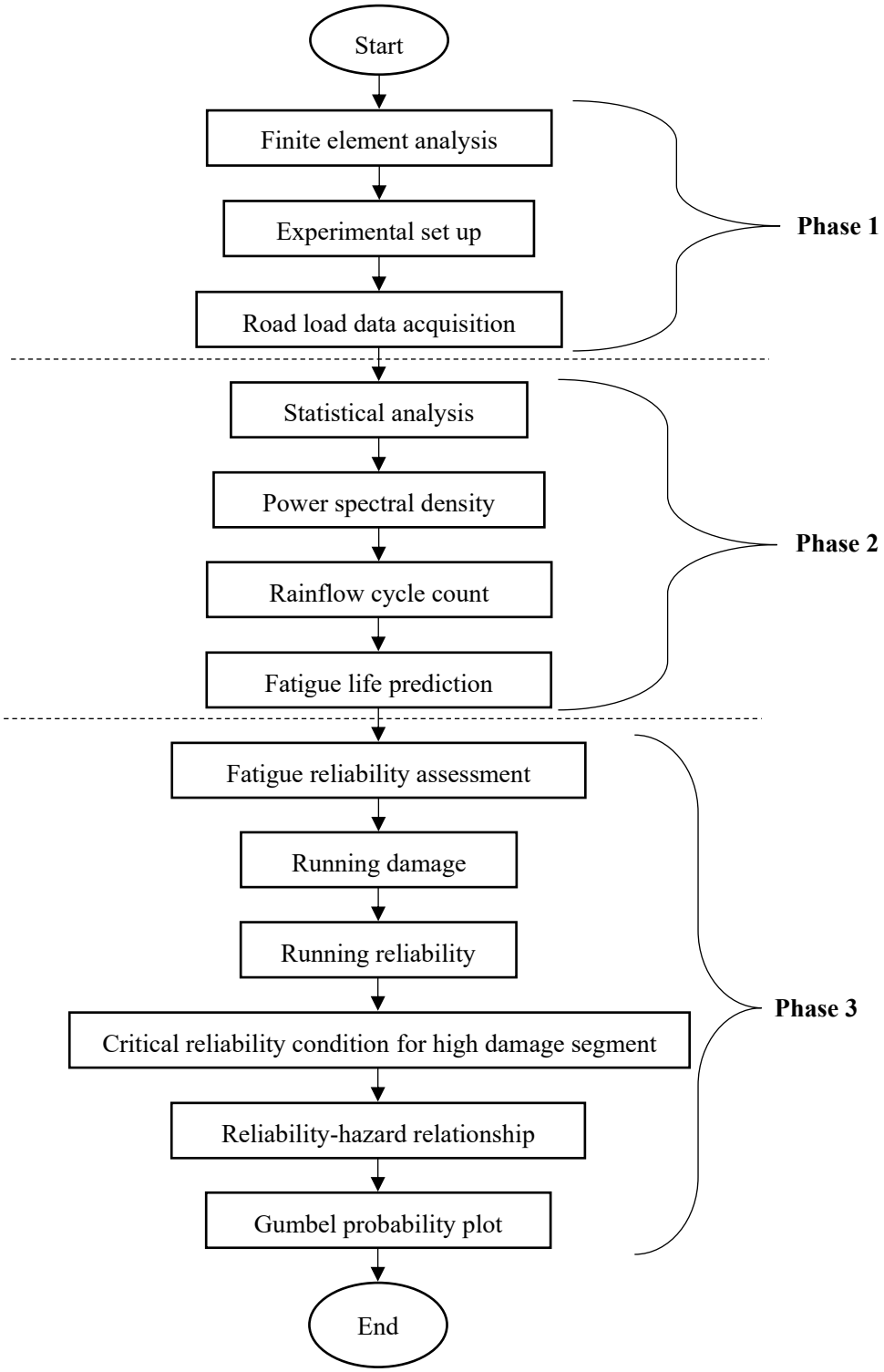

Fig. 1. Process flow for fatigue reliability assessment in modelling a running-reliability technique under random strain loads.

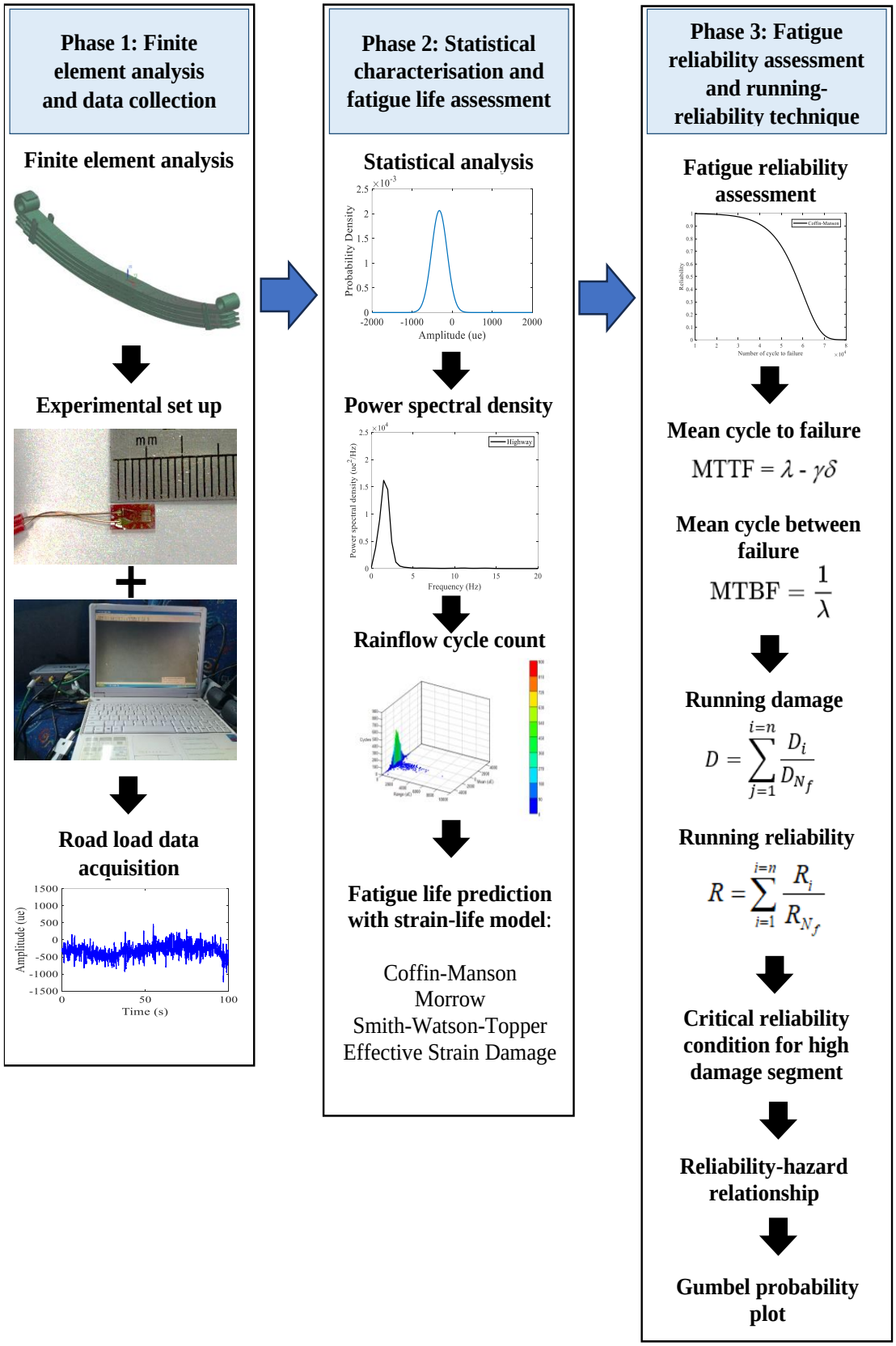

Fig. 2. Methodological framework for running-reliability technique using strain-based loads.

2.1. Phase 1: Finite element analysis and data collection

As an initial step, the finite element analysis (FEA) used a commercial software, Simcenter™ 3D, to model and measure the hotspot or critical region on a leaf spring component. This is important as it will provide the critical region of the

suspension to the various strain load data of the strain gauge from the data acquisition system. The conventional techniques for FEA are geometry, mesh, material and properties, load applied as well as boundary condition. The model of leaf spring geometry is modelled with a 2mm mesh size 3,923,712 nodes and 5,925,096 elements of three-dimensional (3D) with isoparametric tetrahedron mesh elements. Fig. 3 presented a leaf spring geometry with a fine mesh size of 2 mm. The 2 mm mesh size was selected as the best mesh size in this study with subjected to a mesh convergence analysis, as shown in Fig. 4(a). Fig. 4(b) shows the percentages of error between 2 mm to 10 mm mesh size, where the minimum of error is 2%. For the boundary condition, force was set in *z*-axis at the centre of the leaf spring as displayed in Fig. 3. In this assessment, the leaf spring is considered as a whole structure that assumes friction coefficient is zero. This is because the purpose for finite element analysis is to determine the critical region in order to determine hotspot to put strain gauge to capture strain data under maximum deformation and von-Mises stress. The force applied was set as a on the leaf spring geometry is equivalent to a quarter of the total weight mass of a vehicle. The total weight of a bus is 10,570 kg. The one eye was set as a fixed rotated constraint, while the movable constraint was set on the other eye at *x*-axis. The SAE 5160 carbon steel material was utilised in FEA as a leaf spring is commonly made a carbon steel of SAE 5160 [26]. The mechanical properties for SAE5160 carbon steel are as follows: the ultimate tensile strength, S_u of 1584 MPa, a yield strength, S_y is 1487 MPa, a modulus of elasticity, E is 207 GPa, and Poisson ratio is 0.27.

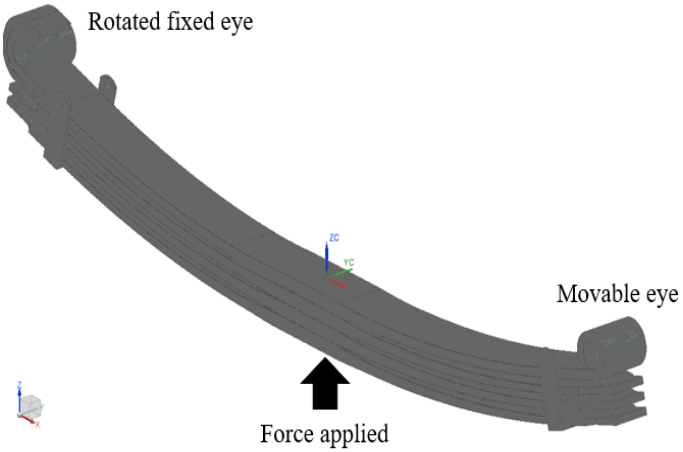

Fig. 3. Leaf spring geometry with 2 mm mesh size.

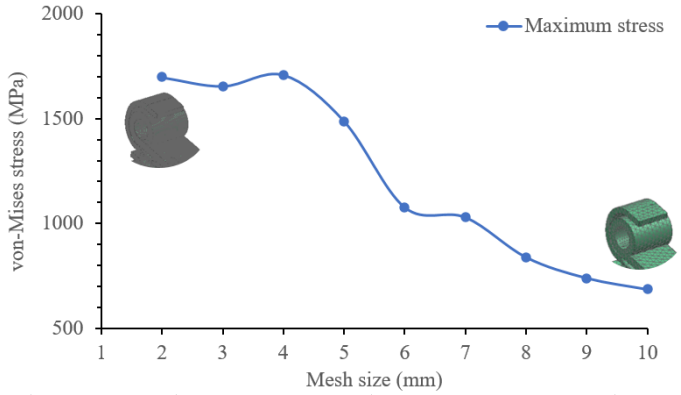

(a)

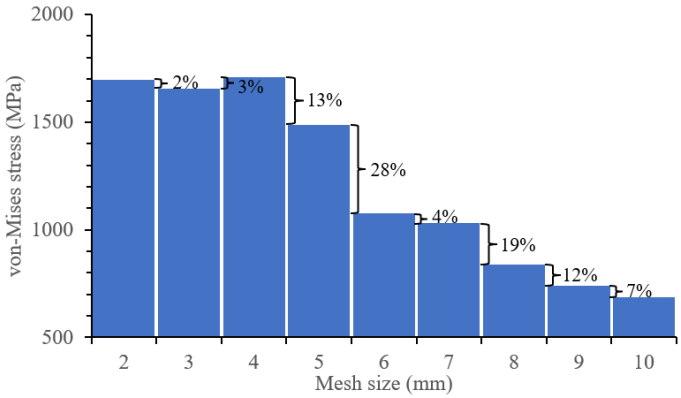

(b)

Fig. 4. (a) Mesh convergence analysis; (b) percentage of error.

2.2 Road load data collection for fatigue life evaluation

The leaf spring component for an express bus was used to collect the random strain loading at various road conditions as displayed in Fig. 5(a). The strain gauge is fixed on a master leaf spring at the critical region according to the results collected from the FE analysis (Fig. 5(b)). A critical region from the FE model was used to capture the strain data as this provides the maximum von-Mises stress dan maximum deformation. This is also mentioned by Kong et al. [26] when assessing the fatigue life prediction of parabolic leaf spring under various road conditions. The data acquisition system of Somat eDAQ was then connected from a strain gauge and linked to a laptop to collect and display the signal extraction, as shown in Fig 5(c). A sampling data was set to 500 Hz which was satisfactory to obtain all the information needed in the data extraction for automotive components [27]. The maximum bandwidth must below than 500 Hz to ensure a quality control is not affected [28].

To extract various random loads, the vehicle travelled on three types of road profiles: a highway with a smooth condition,

rural road with potholes features, and a campus route in Universiti Kebangsaan Malaysia that involved a bumps profile. The standard of ISO8608 was fulfilled as for the road surface of rough level for a road test [29]. The bus was driven at a speed range of 70 – 80 km/h on the highway route, 50 – 60 km/h on the rural route, and 30 – 40 km/h on the campus route. As for a speed range for vehicle on Malaysian roads was subjected to the National Speed Limit Order 1989 [30]. The routes for the road test were at a distance ranging from 3.7 to 8.1 km (Fig. 5(d)).

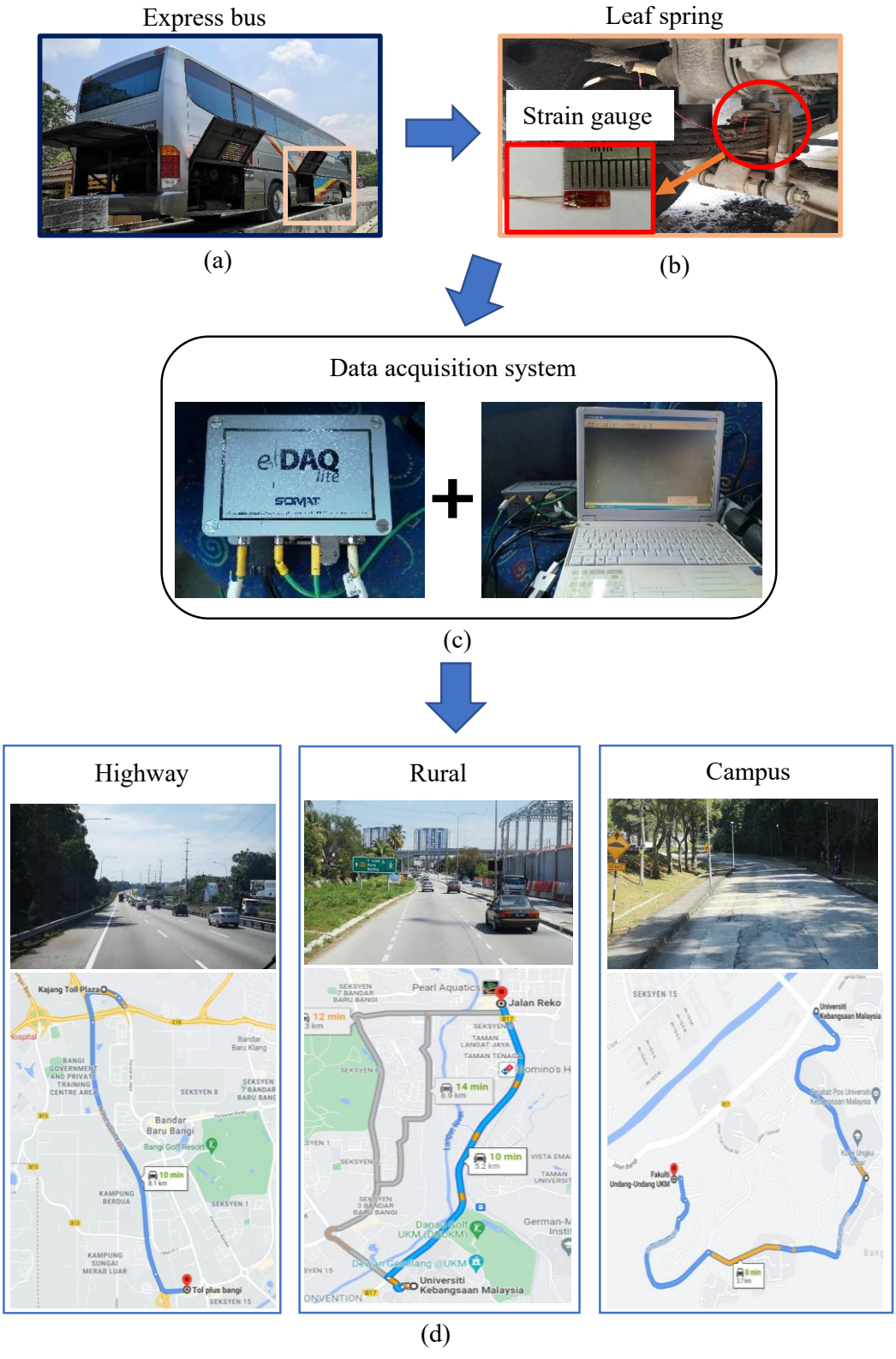

Fig. 5. Experimental set up for random strain data collection.

2.3 Statistical characterisation based on the captured road load signal

The statistical approach has been used to generally associate fatigue failure of a component or structure, particularly in characterising damage behaviour and damage monitoring [31] under the variable amplitude loadings. Parameter of global statistical such as mean, standard deviations (SD), root-mean-square (rms) and kurtosis are typically can be applied to characterise structural damage. The general probability plots namely as probability density function (PDF) and cumulative density function (CDF) also been implemented in identifying the failure occurred [32]. The PDF defines the probability behaviour towards time, and CDF determines the failure probability in a specified time interval. For a series of variable amplitude $X(t)$, a PDF (P_X) of Gaussian distribution is expressed as:

$$P_X = \frac{1}{SD\sqrt{2\pi}} e^{\frac{(X-\bar{x})^2}{2(SD)^2}} \tag{1}$$

where $\bar{x}$ is a mean value and SD is a standard deviation value.

In a normal distribution, the mean is the central value of a bell curve in a distributed data. For the n sample of data, the parameter of mean is stated as:

$$\bar{x} = \frac{1}{n}\sum_{j=1}^{n} x_j \tag{2}$$

The amount of dispersion value of a set data is defined as the standard deviation (SD). Thus, the SD is stated as:

$$SD = \left\{\frac{1}{n}\sum_{j=1}^{n}\left(x_j - \bar{x}\right)^2\right\}^{\frac{1}{2}} \tag{3}$$

In the time-domain, the energy distributed in a signal can be described using a root-mean-square (rms) parameter [12]. For the rms of n data size is stated as:

$$rms = \left\{\frac{1}{n}\sum_{j=1}^{n} {x_j}^2\right\}^{\frac{1}{2}} \tag{4}$$

To determine that a sample data is a stationary or non-stationary time series, the kurtosis parameter is calculated based on the peak in a sample data. If a value of kurtosis is exceeding 3.0 in Gaussian distribution, the data is considered as a non-stationary because of the excitation peaks involvement in a time series data. It also may refer to damage occurred for a component or structure [33].

$$K = \frac{1}{n(rms)^4}\sum_{j=1}^{n}\left(x_j - \bar{x}\right)^4 \tag{5}$$

Subjected to frequency domain, the vibration of a random loading in repeated times collected by the acquisition system is non-stationary data [34]. In a random vibration analysis, a common method to determine a signal in frequency domain is named as power spectral density or PSD. In fatigue analysis, it defined an energy content in a signal that led to fatigue damage appeared. The PSD indicated as an essential PSD for a signal, $S(f_k)$ and the frequency of harmonic, f_k, is given by:

$$A_k = \sqrt{2\Delta f \cdot S(f_k)} \tag{6}$$

The Δf denotes as a frequency resolution, which explains the spacing between data points in frequency domain.

The PSD defines the frequency trend of high and low in an energy unit per frequency, $\mu\varepsilon^2/Hz$, which describes the energy intensity that distributed in a signal [35]. There are two methods in obtaining the PSD result: the fast Fourier transform approach and the computed autocorrelation function conversion. These approaches are acceptable to determine the PSD, particularly for random amplitude loading.

2.4 Fatigue life approaches using common strain-life and load cycle sequence models

As for fatigue life assessment, the common strain-life method is normally applied in calculating a fatigue life by involving a plastic deformation that appears in fatigue cyclic loading [36]. The rainflow counting algorithm is utilised in predicting fatigue life as for defining an equivalent number of cycles. A fatigue cyclic loads is a loading and unloading in time series as shown in Fig. 6(a). In each cycle, the maxima and minima are significant in calculating fatigue life. The average data point where not significant between maxima and minima will be removed in fatigue life calculation, that been demonstrated in Fig. 6(b) and (c) [37].

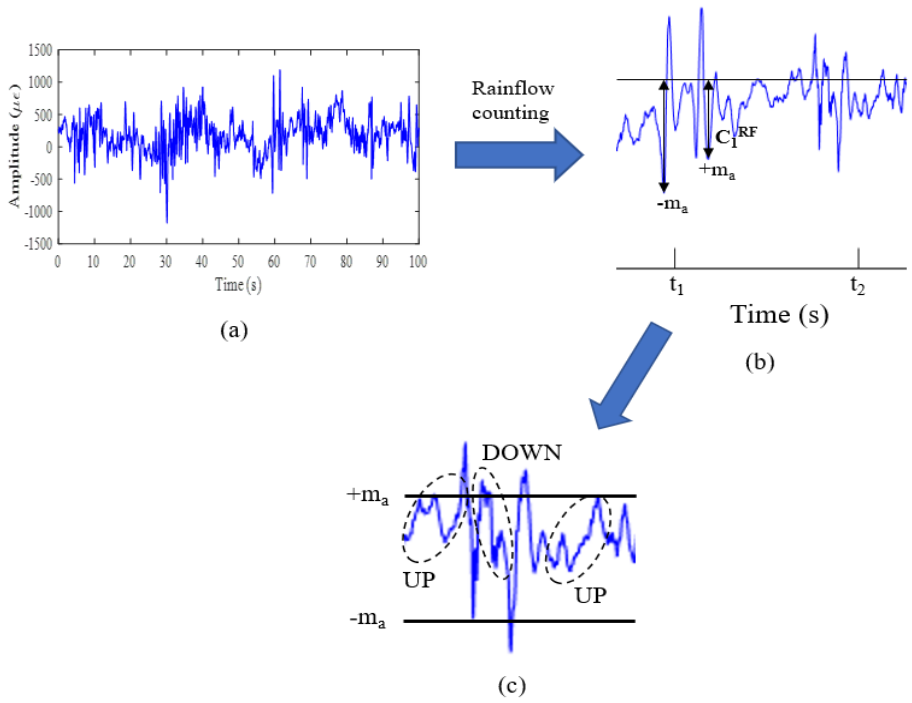

Fig. 6. Rainflow counting method from random loading on the leaf spring.

The Coffin-Manson approach generally proposed for a number of cycles prediction in low cycle fatigue and strain amplitude in uniaxial [38]. This model excluded the mean stress effect for certain alloys and metals that consider in the fatigue life. The Coffin-Manson model proposed the elastic and plastic forms was included in equation below:

$$\varepsilon_a = \frac{\sigma'_f}{E}(2N_f)^b + \varepsilon'_f(2N_f)^c \tag{7}$$

where ε_a is the total sum of strain amplitude, E is modulus of elasticity, σ'_f is the coefficient of fatigue strength, ε'_f is the coefficient of fatigue ductility, b is the exponent of fatigue strength, c is the exponent of fatigue ductility, and N_f is the fatigue life.

With subjected to a compression and tension loads during operating condition, the effect of mean stress was included as proposed in Morrow as well as Smith-Watson-Topper (SWT) approach. The mean stress, σ_m is calculated by the mean of minimum and maximum peak under tensile and compressive stresses, resulting to a significant effect on fatigue behaviour and deformation. For the SWT model, the effect of mean stress is calculated as the tensile stress of maximum, σ_{max} and strain amplitude [39]. The Morrow and SWT models are addressed in Eq. (8) and (9), respectively, as:

$$\varepsilon_a = \frac{(\sigma'_f - \sigma_m)(2N_f)^b}{E} + \varepsilon'_f(2N_f)^c \tag{8}$$

$$\sigma a \frac{(\sigma'_f)^2}{E} \quad {}^{b} \quad {}^{c} \quad {}_{f} \quad {}_{f} {}_{f_{f\ max}} \tag{9}$$

The extensive model of strain-life fatigue damage considers the load cycle sequence effect called effective strain damage (ESD), which was developed by Abdullah, and it was suggested a better enhancement [14]. The method in acquiring the cause for crack growth and crack closure has functioned properly for several materials, geometries of component, mean-strain effects, load spectra, and magnitudes of strain. As assumption in this model, the parameter of fatigue damage as the described as follows:

$$E\Delta\varepsilon^* = A(N_f)^B \tag{10}$$

The $\Delta\varepsilon^*$ is the size of total effective strain for a closed hysteresis loop connected to crack growth of fatigue. A and B are the constants of material. The size of $E\Delta\varepsilon^*$ defined as a particular cycle is a function of opening crack stress, S_{op} level, and this point is a previous to a stress and strain size within the load history. The previous calculation is improved as given:

$$E\Delta\varepsilon^* = E(\varepsilon_{max} - \varepsilon_{op}) - E\varepsilon_i \tag{11}$$

where, ε_{max} is a maximum strain and ε_{op} is an opening crack strain of a particular cycle, while ε_i is the strain range of intrinsic fatigue limit according to variable amplitude loading. With consideration the sequence of cycle impacts, a parameter of decay, m, is utilised in ensuring the modification in stress of

opening crack in two adjoining cycles. ΔS_{op} is addressed as given:

$$\Delta S_{op} = m(S_{ss} - S_{cu}) \tag{12}$$

where S_{cu} is the opening stress of current, that indicated as the S_{op} value of the previous cycle. S_{ss} is the opening stress of steady-state. The parameter of m can be obtained in a data series of failure tests [40]. S_{ss} is addressed as given:

$$\Delta S_{ss} = \alpha S\left(1 - \left(\frac{S_{max}}{S_y}()\right)()_{min}\right)_{max} \tag{13}$$

where α and β are the constants of material, S_{max} is the stress of maximum from an earlier higher cycle, S_{min} is the stress of minimum from an earlier higher cycle, and S_y is the yield stress of cyclic [14].

As for fatigue life (N_i), the particular cycle is given as:

$$N_i = (E\Delta\varepsilon */A)^{\frac{1}{B}} \tag{14}$$

2.5 Linear Damage Assessment

In variable loading, the linear damage rule can be used in calculating a fatigue damage. The Palmgren-Miner (PM) technique calculates the amount of fatigue damage dividing with entire cycles included. Thus, the fatigue damage or D is measured as given:

$$D = \sum \frac{n}{N_f} = 1 \tag{15}$$

where n is the total of cycle calculated in an individual range of mean and strain. The PM rule normally utilised by referring to the easy method and accurate which can be implemented in the rainflow cycle counting method, especially involving a random loading data [41]. Subjected to a sequence of load cycle method, the effects are included in fatigue life evaluation since the parameter of crack closing depicted a stress decay rate overloading. Therefore, the rule of PM possible to be assessed by using the evaluated sum damage for the ESD model [42].

2.6 Fatigue reliability characterisation for the random road load test

In probabilistic, the Akaike Information Criterion (AIC) is a method to determine the suitable distribution to be used on an analysed dataset. [43]. The smallest value of AIC is said to be the best distribution selected. AIC method is calculating by selecting a minimum negative likelihood value with subjected to the number of parameter, as given as:

$$\text{AIC} = -2\,(\text{Log–likelihood}) + 2\text{k} \tag{16}$$

where k is the number of parameters for distribution model. This technique is useful in measuring a suitable distribution under random dataset. Additional method used in defining the best distribution is a normality test. Commonly, the Anderson-Darling test is utilised to measure the goodness of fit, where a p-value closer to 1 means the fit is better. If the p-value is lower or equal to 0.05, the fit is not accepted [44-45].

In this study, fatigue reliability is based on the Gumbel distribution which lead to the features of high amplitude excitation obtained from the time-domain strain signals. This feature contributes to a failure of the component or structure [46]. Fixed sequences of data set are accumulated in a form data series and repeatedly in multiple times, where the maxima value in each sequence obeys the Gumbel distribution for the number of cycles to failure with CDF, ($F(N_f)$), and is given by the following:

$$F(N_f) = e^{-e^{-(N_f-\lambda)/\delta}} \tag{17}$$

where λ and δ is the parameters of location and scale, respectively [47]. The Gumbel distribution parameters are given by the location of $-\infty < \lambda < \infty$ and scale $\delta > 0$.

The mean of Gumbel distribution, also has been referred as the MTTF or mean time to failure is expressed as follows:

$$Mean = \lambda - \gamma\delta \tag{18}$$

where γ is 0.5776, as the constant of Euler's.

PDF for the Gumbel distribution, ($f(N_f)$) is given by the following:

$$F(N_f) = \frac{1}{\delta}e^{\left(\frac{N_f-\lambda}{\delta}+e^{-\left(\frac{N_f-\lambda}{\delta}\right)}\right)} \tag{19}$$

The hazard function, $h(N_f)$ is specified in the Gumbel distribution as follows:

$$h(N_f) = \frac{1}{\delta}e^{-\left(\frac{N_f-\lambda}{\delta}\right)} \tag{20}$$

The reliability, $R(N_f)$ is given in the Gumbel distribution by the following:

$$R(N_f) = \frac{1}{\delta}e^{-\left(e^{-\left(\frac{N_f-\lambda}{\delta}\right)}\right)} \tag{21}$$

The mean time between failure (MTBF) of a component is calculated from the total simulation time and expected number

of failures. Hence, the MTBF is expressed as:

$$MTBF = \frac{1}{h(N_f)} \tag{22}$$

The probabilistic approach using the Gumbel distribution is widely applied to the of extreme data model such as random or big data set, which concentrates on the application of severe values in engineering issues. For this reason, the Gumbel distribution is beneficial to estimate the possibility of extreme challenges that might appear [48].

2.7 Running-reliability for risk monitoring for random road loads

In a fatigue reliability assessment, the reliability distribution is determined in terms of time series. This technique is called time-reliability histories where the accumulated reliability is distributed through time. Hence, time-reliability data to represent the reliability for each cycle can be implemented for the strain load data. This technique is the running-reliability based on the reliability history for risk monitoring in time-domain [49].

The reliability was computed for each peak-valley cycle. In order to determine the running-reliability, Eq. (22) was derived in a time series based on the method of PM linear damage rule:

$$R = \sum_{i=1}^{i=n} \frac{R_i}{R_{N_f}} \tag{23}$$

where R_i is the reliability a in every cycle and R_{N_f} is the reliability for number of cycles to failure. The rate of reliability will increase if fatigue damage is on high value. Thus, the reliability is at a good rate when fatigue life is at a lower value.

3. Results and discussion

3.1 Finite element analysis under static load

FEA was conducted to determine a hotspot or critical contour on a model of automotive component. The load applied for vehicle specifically on the FE model was 25.914 kN, where converted from a total weight of the vehicle being 10,570 kg. In order to apply the load on a leaf spring, the total mass was divided by 4. The maximum deformation was shown at 22.83 mm at the U-bolt area as displayed in Fig. 7(a). However, the von-Mises stress concentration achieved 613.57 MPa at the critical contour, as illustrated in Fig. 7(b). This result was used to determine the location to fixed a strain gauge. The maximum von-Mises was obtained at 920.36 MPa, where it was found to be lesser than the ultimate tensile strength of 1584 MPa. As a result, this is applicable to determine the hotspot or critical region.

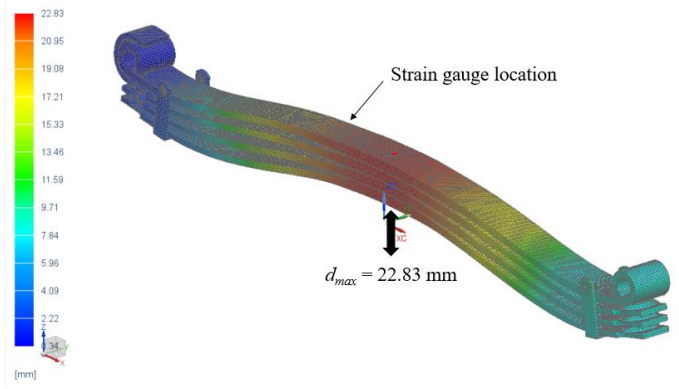

(a)

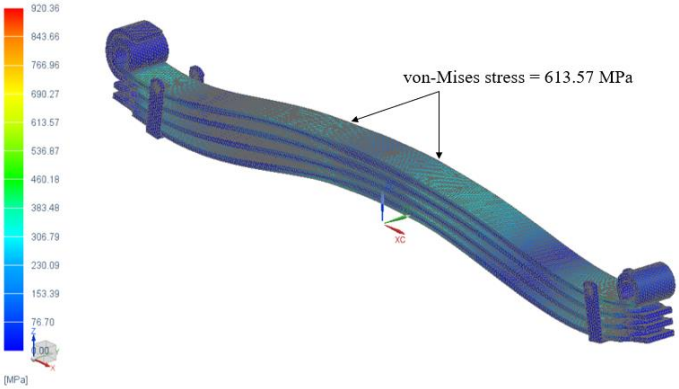

(b)

Fig. 7. (a) leaf spring deformation and (b) von-Mises stress.

3.2 Statistical features characterisation of the road loads in time-frequency domain

The entire strain road loads include various road condition were extracted in 300 s at a 500 Hz rate of sampling, capturing 150,000 discrete data points. Fig. 8 displayed a time history and PDF plot for entire road load condition which involves highway, rural dan campus data, with a duration of 100 s for each road types over a total of 300s for entire time histories. As for various strain road loads in duration of 100 s that obtained 50,000 discrete data points. Fig. 9 illustrates the time histories and PDF plot for highway (smooth), rural (potholes), and campus (bumpy) road conditions. The time histories plot showed the campus route data included many high excitations amplitude in contrast with the rural and highway route data. This was due to uneven and bumpy surfaces that contributed to high amplitude excitations, and it was considered as heavily non-stationary data that were subjected to high amplitude events as circled (black) in Fig. 9(b) and 9(c). In contrast, the highway data showed

mildly nonstationary behaviour due to the smoother highway surface and less braking condition. The highest amplitude range for highway, rural, and campus was 462.9 to -1235.9 $\mu\varepsilon$, 578.6 to -965.85 $\mu\varepsilon$, and 1186.9 to -1180 $\mu\varepsilon$, respectively.

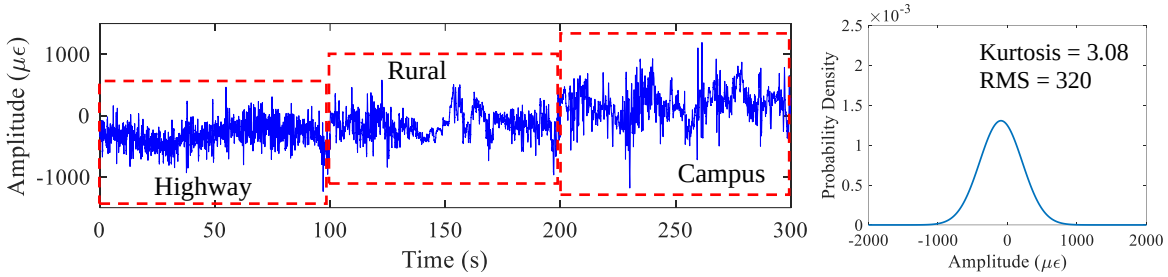

Fig. 8. Time history and PDF for entire road load conditions.

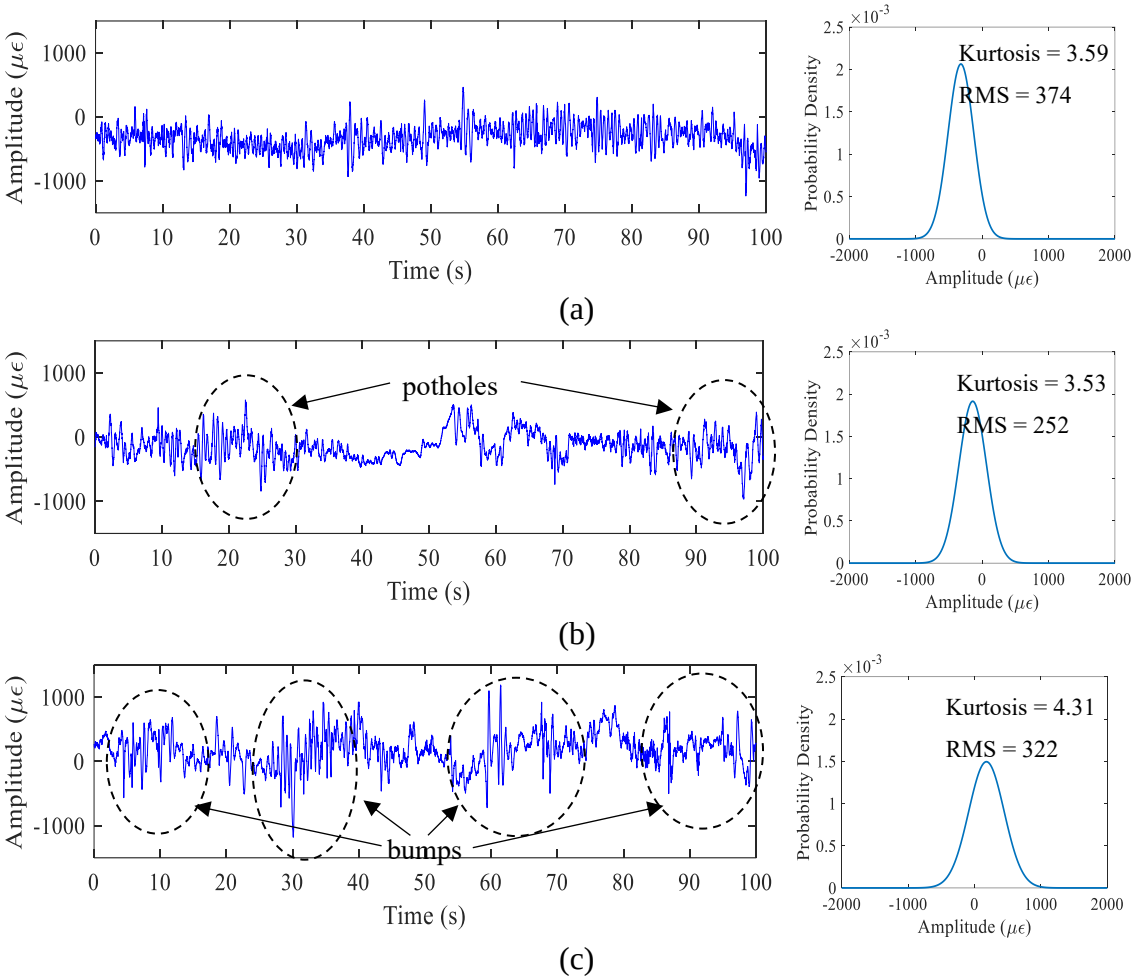

Fig. 9. Time histories and PDF for (a) highway; (b) rural; and (c) campus.

Statistically, the PDF and global statistical parameters were implemented to characterise the random data behaviour. The PDF plot highway data presented a narrow curve bell shape as compared to the rural data. In contrast, the campus data presented the broadest curve bell shape. The shape of the bell curve was determined by the standard deviation. The highway, rural, and campus data produced an SD value of 193 $\mu\varepsilon^2$, 208 $\mu\varepsilon^2$, and 267 $\mu\varepsilon^2$, respectively. The high amplitude excitations might influence the SD values. The value of mean locates the peak of PDF curve where the results exhibited the mean values are -320 $\mu\varepsilon$, -142 $\mu\varepsilon$ and 180 $\mu\varepsilon$ for highway, rural, and campus, respectively. As for entire data, the SD and mean values are 306 $\mu\varepsilon^2$ and -94 $\mu\varepsilon$, respectively. The positive and negative mean values are described as the automotive spring under tension and compression conditions according to vibration loading [50].

Subjected to kurtosis value, the highway data obtained a kurtosis value of 3.59, rural data at 3.53, and campus data at 4.31. The kurtosis value from the campus data was the highest among others, describing the spikiness of the data. Therefore, the campus significant data result included mostly high

amplitude excitations by comparison with the rural and highway data. The kurtosis from the rural data was lesser than the highway data, and it might cause high amplitude excitations: a leaf spring experienced less absorbed vibrations due to a few conditions related to braking or a vehicle moving at low speed. The rms value showed the highway, rural, and campus data produced 374 $\mu\varepsilon$, 252 $\mu\varepsilon$, and 322 $\mu\varepsilon$, respectively, indicating the contained vibration energy of highway data achieved the highest rms value. This is due to the amplitude excitation in a medium-range that constantly contributed to a higher vibration energy in the random data, whereby it explains the range of minimum to maximum strain amplitudes from highway is higher than values from rural.

Subjected to domain of frequency, the PSD was applied in determining an internal vibration energy in the data distribution of a random strain loads. Fig. 10 illustrates the PSD for different road condition data. As a result, a campus data produced to be the higher energy of vibration by obtaining 2.01×10^4 $\mu\varepsilon^2/Hz$, as compared to the highway data (1.62×10^4 $\mu\varepsilon^2/Hz$) and rural data (1.2×10^4 $\mu\varepsilon^2/Hz$). This PSD responses defined a campus data included many high excitation amplitudes that caused fatigue damage. The distributed vibration energy for a leaf spring was around 5 Hz, which indicates the damage occurred at a range of low frequency. By referring to frequency analysis, an automotive suspension component can be achieved a high amplitude of PSD which the frequency bandwidth is below than 10 Hz [51].

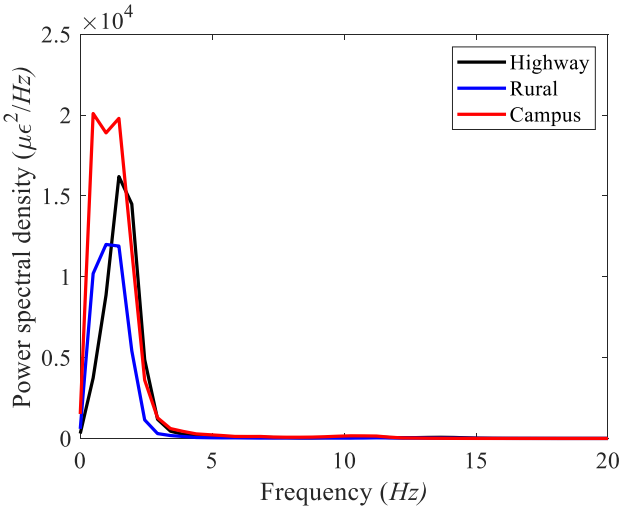

Fig. 10. Power spectral density for different road conditions.

3.3 Assessing the Rainflow cycle counting from the strain signal

The method of rainflow cycle counting was exploited to define fatigue life for the purpose in minimizing a various strains spectrum to the reversal set of strains in terms of time domain. Fig. 11 exhibits a rainflow counting method for various road data. The campus data provided the highest cycle count of 704 cycles, followed by rural (669 cycles) and highway data (489 cycles). The campus data also exhibited a blue contour that was scattered at the highest range against to the rural and highway data that lead to the high amplitude excitations influencing the peak and valley estimation. The strain cycle was scattered in negative and positive mean regions, explaining that a leaf spring is under tension and compression conditions along operating service.

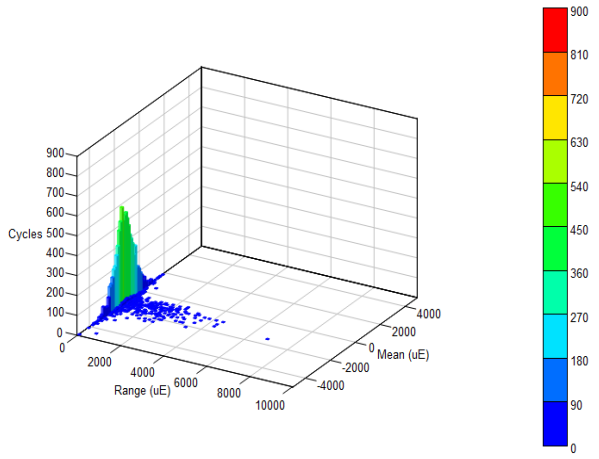

(a)

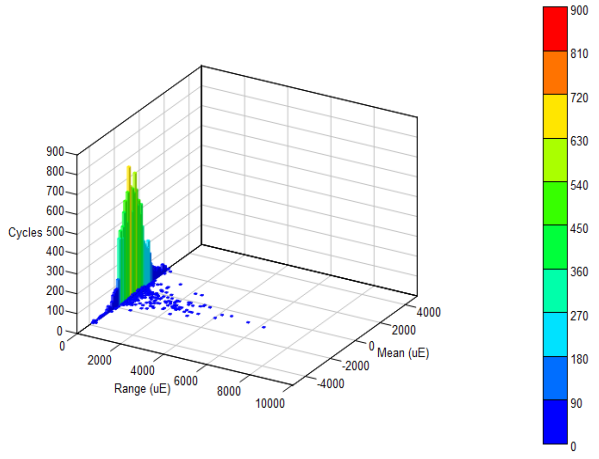

(b)

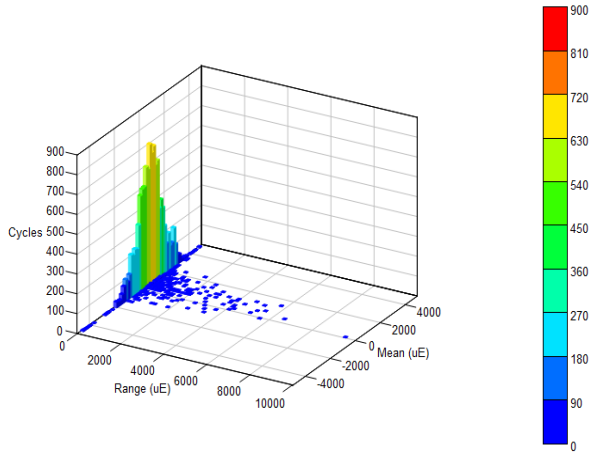

(c)

Fig. 11. Rainflow counting for (a) highway; (b) rural; and (c) campus.

3.4 Fatigue life prediction from the various road load test

The fatigue life was evaluated according to the model of strain-life including Coffin-Manson, Morrow and SWT, as well as the ESD model load cycle sequence based. The used of ESD model was to calculate the fatigue life assessment according to the cycle sequence effect which could also be used for random loading [11]. Fig. 12 illustrates the evaluated fatigue life for various strain-life models. It presents the rural data achieved the higher fatigue life, as against the highway and campus data for strain-life models. Regarding to entire road data, a fatigue life is the lowest, and this is due to high range of minimum and maximum strain amplitude in the entire data. With respected to the model of strain-life, the SWT model obtained the higher fatigue life data for the highway and rural data while the campus data had the lower fatigue life. The leaf spring under compression and tension conditions contributed the fatigue life span during operating condition. In contrast, the ESD model displayed the highway data produced the higher fatigue life, as against the rural and campus data. The predicted fatigue life might differ from each model because the Morrow model involved the effects of mean stress of the compression, likewise the SWT models involved the mean stress effect of maximum tensile stress and strain amplitude, while the ESD model according to the effect of cycle loading sequence. This is due to the ESD model more concerned to cycle load sequence effect compared to conventional strain-life models. On the other hand, a campus data obtained the lower fatigue life which was expected lead to the high amplitude excitations that caused a shorter life span.

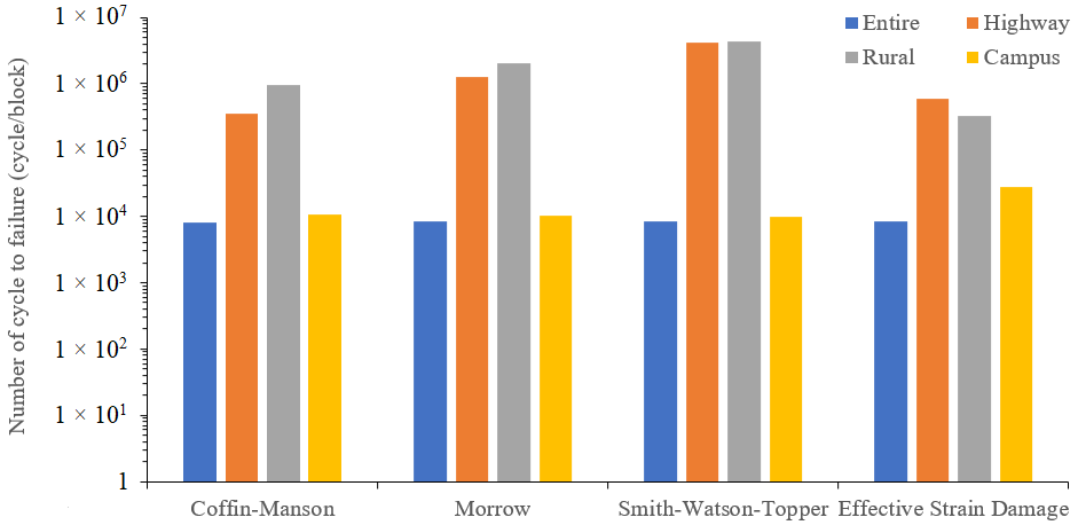

Fig. 12. Fatigue life predicted for various strain-life models.

3.5. Fatigue reliability assessment under extreme value distribution

In defining be approximate distribution to be used in reliability assessment, the AIC need to be assessed priorly based on Eq. (16). Table 1 tabulated the log-likelihood, AIC, and Anderson-Darling (AD) test value for fatigue life based under various road load condition. In this study, the distribution of Normal, Gumbel and Weibull were used to determine the minimum value for AIC method. It shows the Gumbel distribution produces lowest log-likelihood values, while the Weibull achieved the lowest value for AIC. For AD test result, the *p*-value for a highway and campus data provides the highest value for Weibull distribution, while a rural data presents a *p*-value of Gumbel distribution is

highest compared to Normal and Weibull. By considering the fatigue strain-based data under an extreme data, the Gumbel distribution is selected as suitable distribution in reliability assessment. This is due to the Gumbel distribution also has been used in modelling a failure [43] and predicting fatigue failure [52].

Table 1. Probabilistic model estimation based on Akaike information criterion and Anderson-Darling test for various road conditions.

Data	Distribution	Log-likelihood	AIC	AD	*p*-value
Highway	Gumbel	-63.32	131	0.475	0.100
	Normal	-62.75	129	0.584	0.098
	Weibull	-61.14	126	0.303	> 0.250
Rural	Gumbel	-63.15	130	0.263	0.475
	Normal	-62.75	129	0.377	> 0.250
	Weibull	-61.78	128	0.196	> 0.250
Campus	Gumbel	-42.05	88	0.745	0.013
	Normal	-41.42	87	0.804	0.024
	Weibull	-40.90	86	0.763	0.033

In assessing the reliability analysis, the PDF and CDF were analysed to estimate the probability of failure on a leaf spring based on a curved shape. To describe the probability of failure on a leaf spring, the campus data was used as an extreme load data. Fig. 13 illustrates the PDF plot for strain-based fatigue life in time domain. The PDF plot illustrated the narrower bell shape due to fatigue life data that influenced by bumps condition on campus roads. Fig. 14 illustrates the CDF plot for strain-based fatigue life in time domain, in determining the probability of failure for a component or structure. It shows a leaf spring exposed in failure faster due to high amplitude range in campus road under operating condition. It also, the fatigue life prediction involving ESD model achieved the slowest damage that possibly due to the cycle sequence loading effect in identifying the peak and valley in the damage-time history.

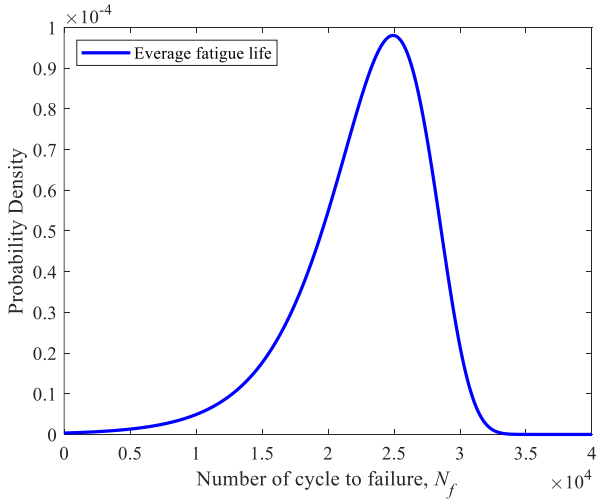

Fig. 13. Probability density function for average fatigue life.

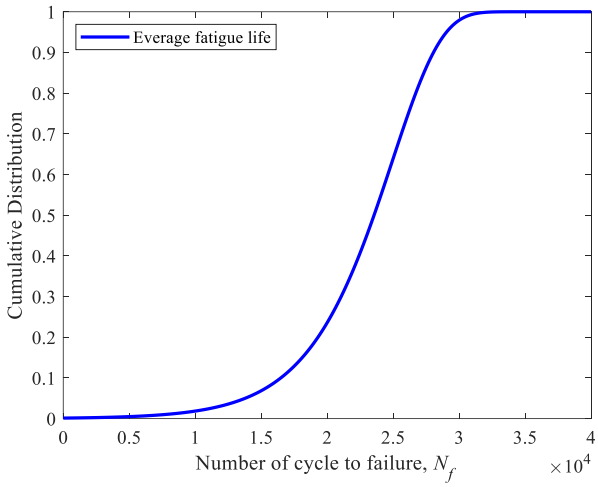

Fig. 14. Cumulative distribution function for average fatigue life.

The reliability was analysed to determine a reliable rate of a leaf spring referring to Eq. (21). Fig. 15 illustrates the reliability plots for strain-based fatigue life in time domain for campus data. Fig. 16 represents the hazard rate for strain-based fatigue life was determined based on Eq. (20). The average fatigue life for campus road revealed that the reliability rate rapidly decreased. In the hazard rate plot, the curve also exhibited the same behaviour where a hazard rate increased rapidly. This is due to a SWT model achieved the lower rate of reliability and hazard, which could be due to the mean stress effect as well as conditions of tension and compression that affected the rates of the leaf spring. On the other hand, the cycle sequence effect of ESD model obtained the failure, which appeared at a higher fatigue life in the reliability and hazard rate.

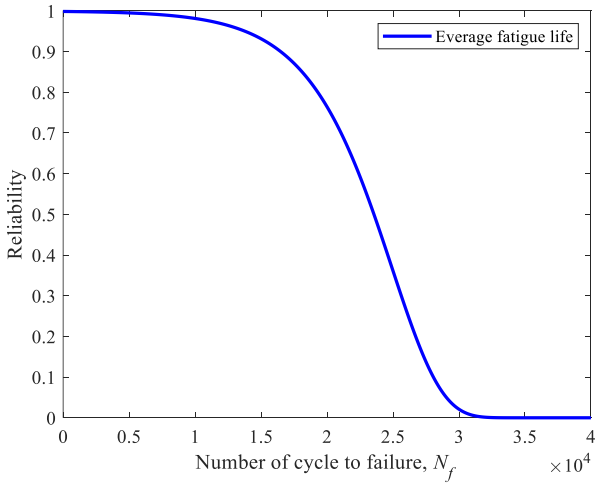

Fig. 15. Reliability for average fatigue life.

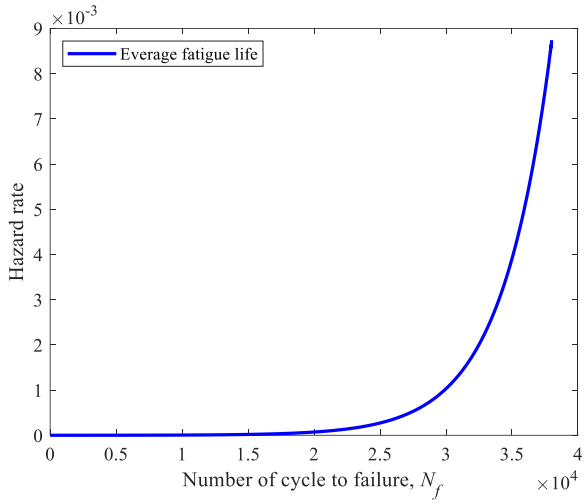

Fig. 16. Hazard rate for average fatigue life.

3.6. Mean cycle to failure, mean cycle between failure and Gumbel probability plot for strain-based fatigue life data

The assessment of fatigue reliability was computed subjected to the fatigue life predicted data using the Gumbel distribution. The mean cycle to failure (McTF) is equivalent to the value of mean for Gumbel distribution based on Eq. (18). Since the fatigue life calculates in cycles unit, thus, this parameter was substituted as a mean cycle to failure [48]. The McTF value for average fatigue life is 2.28×10^4 cycle/block. It estimated that failure could occur before McTF was achieved. In this study, the McTF was calculated to predict the mean cycle of the component that was exposed to failure [53].

The mean cycle between failure (McBF) is represented by the mean time between failure (MTBF) value as the fatigue life is measured in cycles unit [51]. The McBF is used to predict the average cycle between failure of a mechanical component during the in-service period. By using Eq. (22), the McBF plot is portrayed in Fig. 17. The ESD model obtained the highest McBF values compared with the established strain-life models. This may be due to the ESD model which contains detailed information in the load cycle sequence that influences fatigue failure.

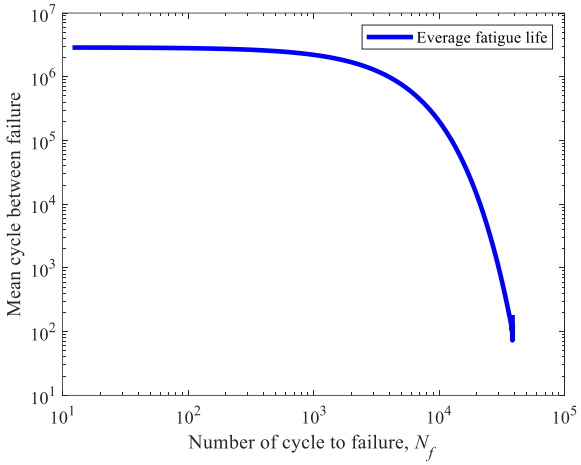

Fig. 17. Mean cycle between failure for average fatigue life.

3.7. Running-reliability for characterisation of fatigue reliability

The technique to monitor the reliability fatigue based in terms of time-domain, the newly model to propose running-reliability based on Eq. (23). To determine the running-reliability, the fatigue damage distribution is defined in time-domain. This newly modelled method is proposed to monitor the risk of failure that might occur on the leaf spring. Figs. 18, 19 and 20 represents the time history, running damage in time-domain, and running-reliability in time-domain for various durability models for the highway, rural and campus data, respectively. As for running damage results, it shows that at a high amplitude, the excitation exhibited the high damage that occurred. The campus data produced the highest damage, and it was significant to the campus data that included many amplitudes of higher range as compared to the highway and rural data. The ESD model showed that the running damage was more detailed where this model rearranged the cycles of rainflow in strain histories based on the time start. The purpose of this rearrangement was to keep the sequence of load cycle effect, which was included into the fatigue life evaluation. As for an established strain-life model, the sequence of load cycle effect

was excluded in their method [14].

The running-reliability technique is modelled by extracting the features of high amplitude excitation obtained from the time-domain strain signals. This is to observe the high damage regions which contributed towards high risk based on the signal features obtained from the road test. The ESD model showed the fatigue life data in time-domain as this model was calculated based on the cycle loading sequence effect where every cycle that had significant fatigue damage was switched to a fatigue life. It was shown that the reliability decreased due to fatigue damage while fatigue life significantly increased. This characteristic can be illustrated in Fig. 21 to define the critical reliability condition for a high damage segment. The ESD model shows the lowest reliability rates of 0.31 which gives the highest fatigue life predicted at 1.15×10^{13} cycles/block. Furthermore, the ESD model tabulates the highest reliability rates of 0.96 at the fatigue life predicted of 1.63×10^{12} cycles/block. The ESD model showed detailed information required in monitoring fatigue failure in time-domain. Thus, the running-reliability technique is suitable to be used in monitoring the risk purpose of a leaf spring failure.

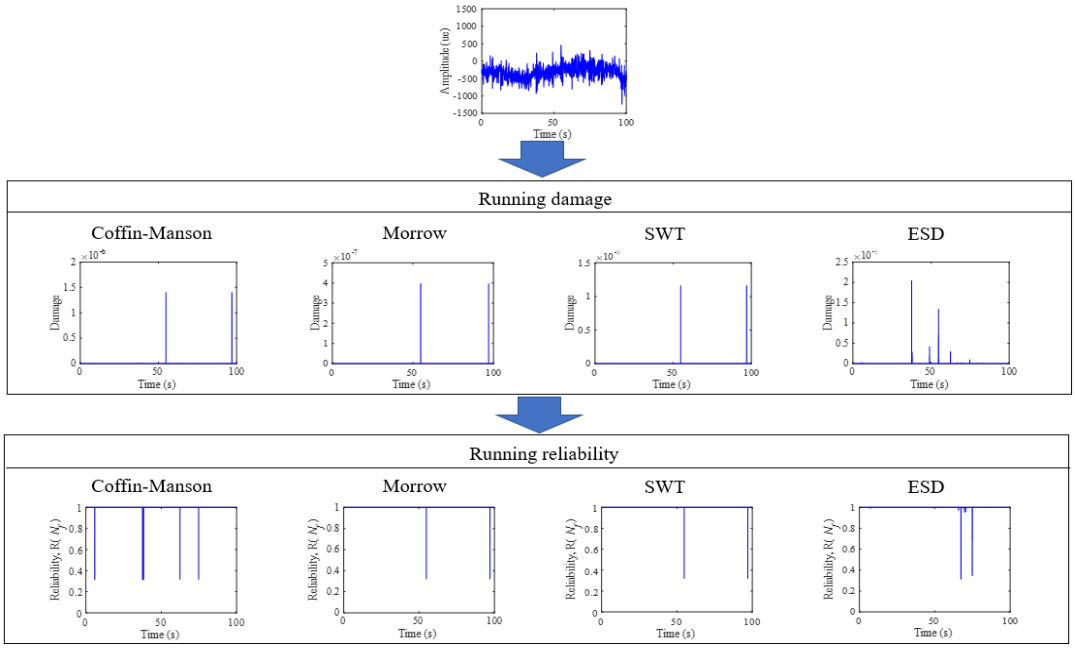

Fig. 18. Assessing the running damage and running-reliability techniques for highway strain loads data.

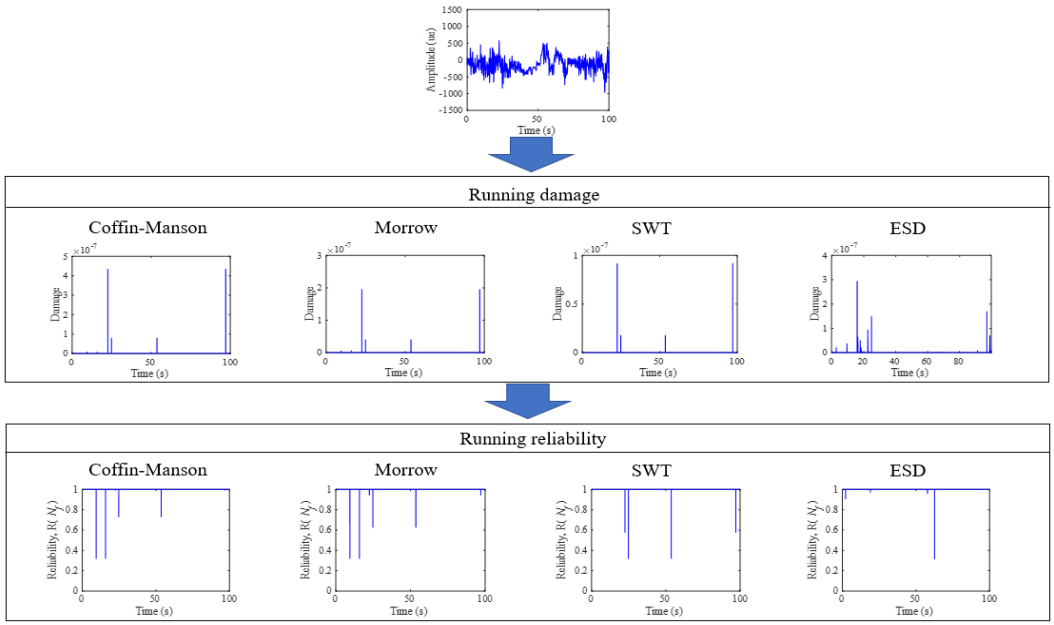

Fig. 19. Assessing the running damage and running-reliability techniques for rural strain loads data.

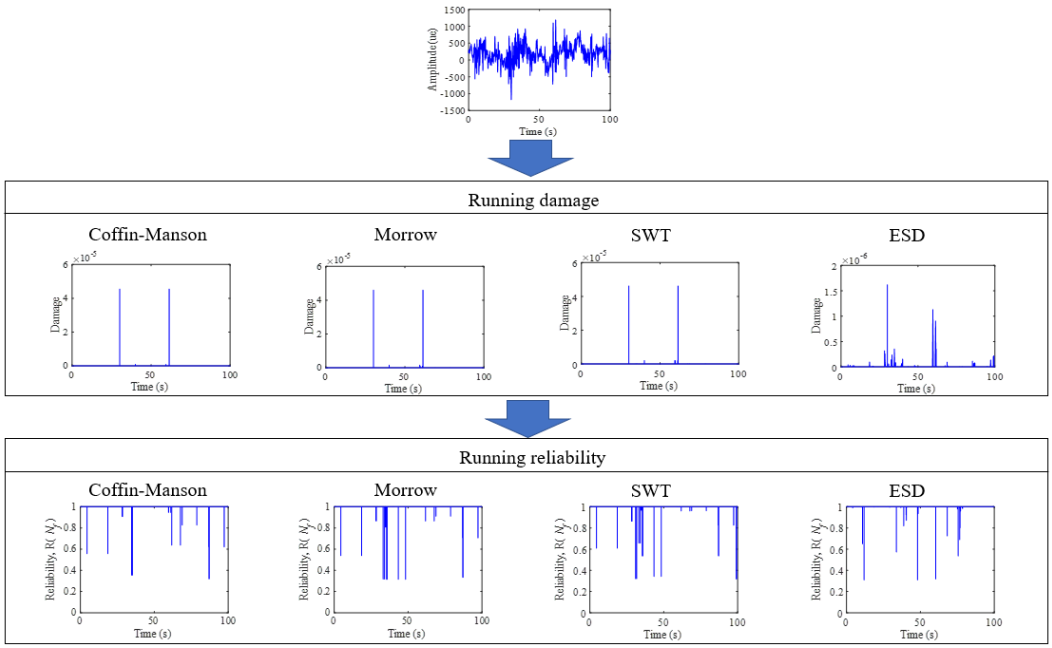

Fig. 20. Assessing the running damage and running-reliability techniques for campus strain loads data.

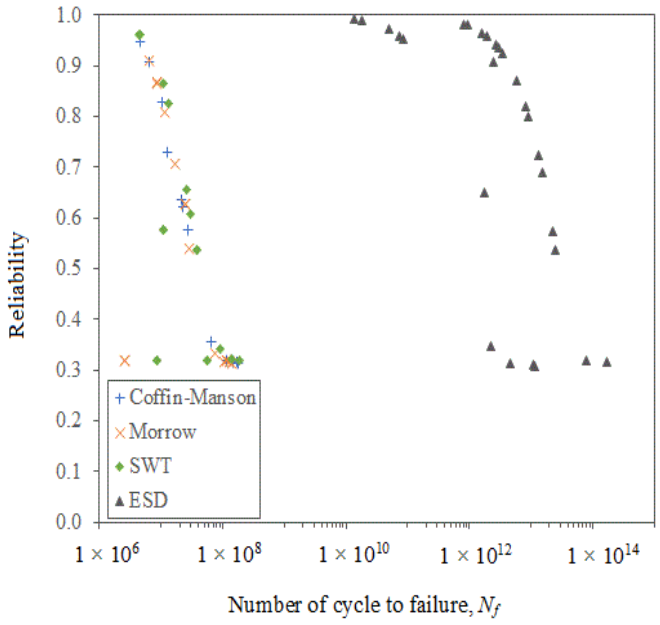

Fig. 21. Critical reliability condition for high damage segment.

3.8. Reliability-hazard relationship under extreme condition for risk monitoring

The reliability-hazard relationship was proposed to determine the risk of a component based on different road loads associated with durability features referring to a failure number of cycles. The rates of reliability and hazard with subjected to cyclic loading that considering the influences of mean stress and sequence of load cycle was represented according to Coffin-Manson, Morrow, SWT as well as ESD models for a campus data as portrayed in Figs. 22 to 25, respectively. The campus data could be represented as extreme data because the data contained mostly high amplitude excitations that described high damage. Fig. 26 illustrates the reliability-hazard relationship concentration. As a result, the fatigue life data were clustered within the 0.70 to 0.90 region. This result was utilised to identify the cycle of life obtained on reliability zone against the failure number of cycles based on the hazard rate extrapolated by using a data of fatigue life. Thus, this method is applicable to identify the concentrated zone of clustering in monitoring a risk to failure.

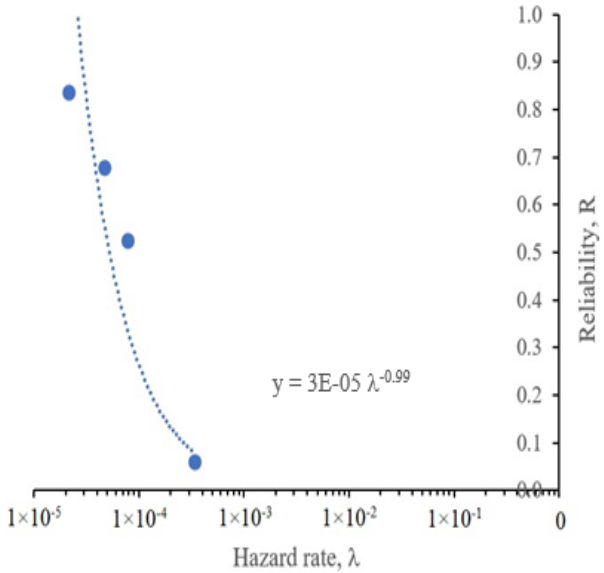

Fig. 22. Relationship of reliability-hazard rate for the Coffin-Manson model.

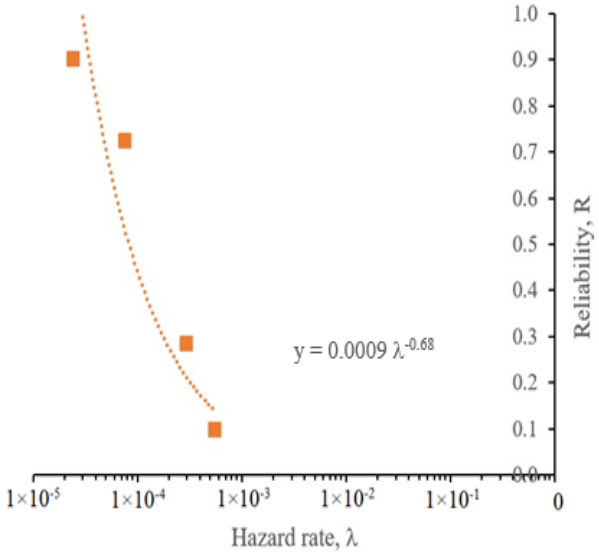

Fig. 23. Relationship of reliability-hazard rate for the Morrow model.

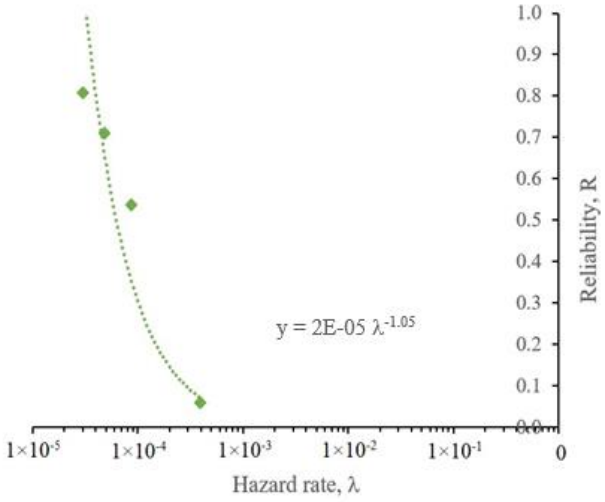

Fig. 24. Relationship of reliability-hazard rate for the SWT model.

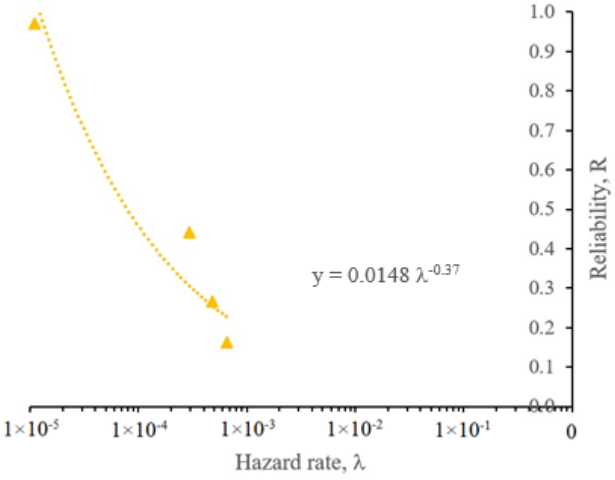

Fig. 25. Relationship of reliability-hazard rate for the ESD model.

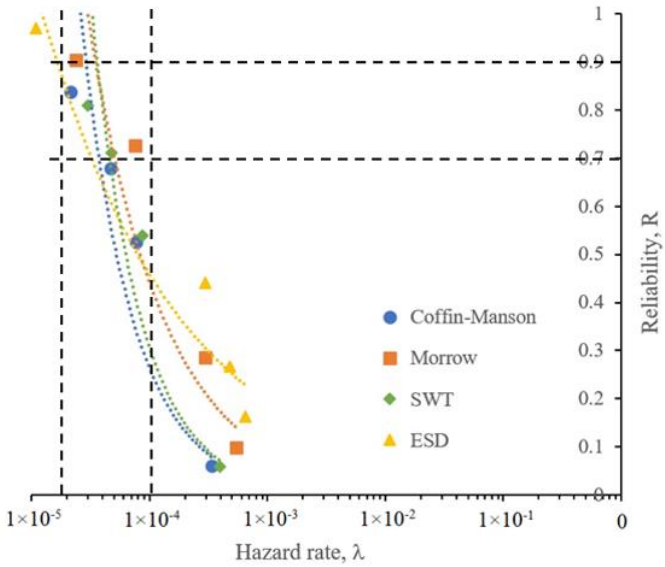

Fig. 26. Reliability-hazard rate concentration.

3.9. Validation of the strain-life model

The distribution of Gumbel has been used in fatigue reliability assessment strain-based to predict the probability of fatigue failure. For this reason, the Gumbel probability plot is required to be done in determining using fatigue life data. Fig. 27 displays the Gumbel probability plot for different strain-life models. The result shows the fatigue life data for the Coffin-Manson model is in a boundary line of 95% confidence level. This is due to the model of Coffin-Manson excluded the effect of mean stress, where a leaf spring experienced compression and tension loads during operating condition. By comparing with each strain-life models, the fatigue life data of a leaf spring is acceptable to use Gumbel distribution because most fatigue life data is within the 95% confidence level.

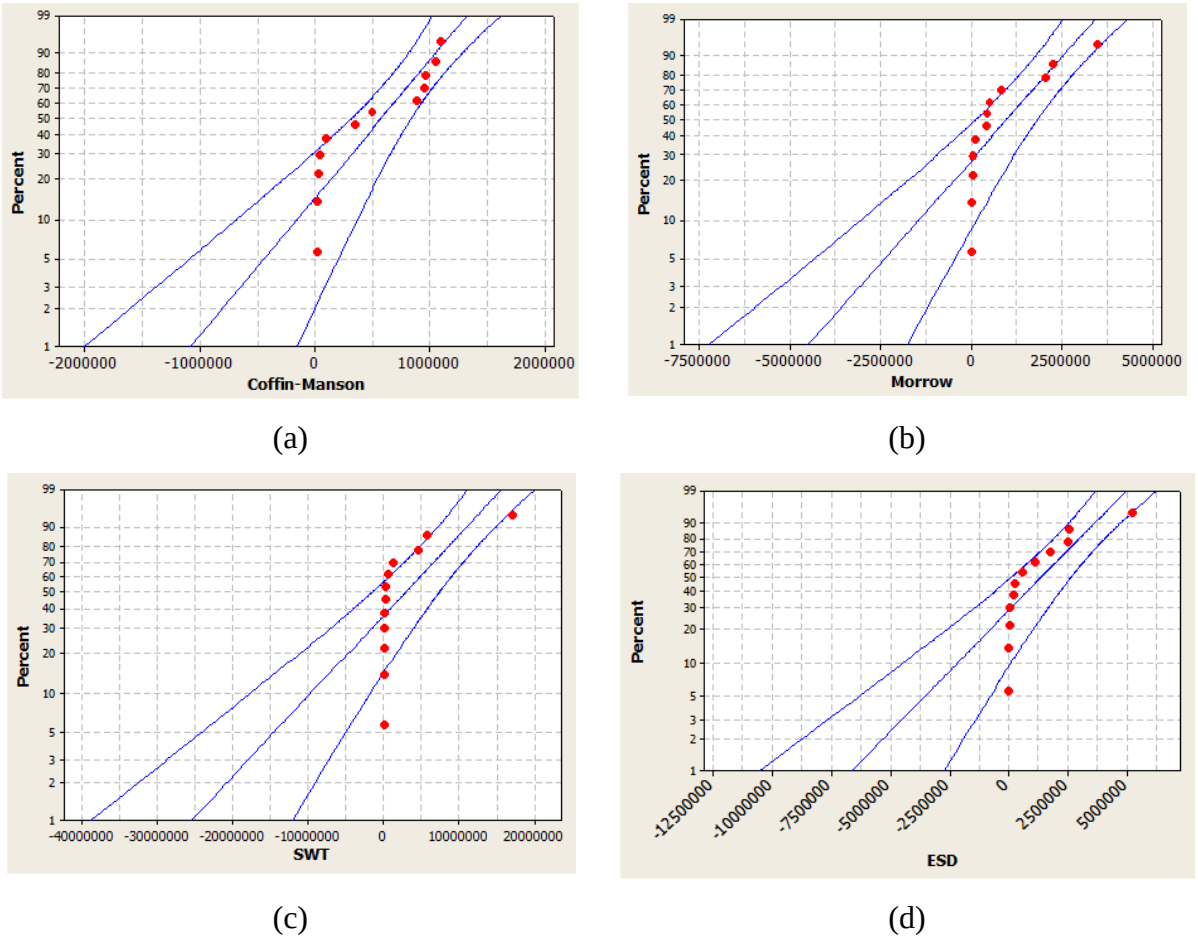

Fig. 27. Gumbel probability plot for: (a) Coffin-Manson, (b) Morrow, (c) SWT, and (d) ESD models.

4. Conclusion

The main purpose of this paper is to use operational reliability technology to monitor the risk of fatigue failure of plate springs to better understand and predict their performance under different road conditions. This study proposed a risk monitoring of fatigue failure on a leaf spring using the running-reliability technique to characterise fatigue reliability assessment subjected to various road loads data strain-based. The FE analysis was implemented on a carbon steel leaf spring geometry to determine the hotspot region for strain gauge installation. In mesh convergence analysis, a percentage of minimum error between mesh size of 2 mm to 10 mm is 2 %. The data collection of a random strain load was subjected to three road profiles where the campus data included numerous high amplitude excitations compared to the rural and highway data because bumps and uneven road surfaces influenced the data behaviour. This characteristic was consistent with the statistical parameter of kurtosis where a data of campus produced the higher kurtosis value at 4.31. The fatigue life assessment is defined according to an established strain-life models of Coffin-Manson, Morrow and SWT including ESD model which considered cycle sequence effect. The ESD model gave the highest range of fatigue life at 2.74×10^4 to 6.07×10^5 cycle/block. The difference between ESD model with conventional strain-life model are around 6 to 13%. The cycle load sequence effect and tension-compression conditions could influence the fatigue life assessment. This study not involving an uncertainty in fatigue analysis; however, it can be considered in future work.

In the reliability assessment, the ESD model revealed that the reliability rate rapidly decreased and it was significant to strain-life models. In consequence to that, the ESD model presented the failure, which appeared at a higher fatigue life in the reliability and hazard rate. The McTF exhibited the range value of 4.32×10^6 to 7.00×10^6 cycle/block. As for McBF, the ESD model presented the highest McBF values compared with established strain-life models. The running-reliability technique showed that high damage occurred at high amplitude excitation, resulting in the decrease of reliability. The reliability indicates

a low rate of 0.31, resulting in a high fatigue life of 1.15×10^{13} cycle/block. On the other hand, this method can be used to monitor the risk of failure for reliability in the time-domain. The reliability-hazard relationship indicated that the fatigue life data are clustered within the 0.70 to 0.90 region. Hence, the running-reliability technique is proposed as a suitable method to monitor the risk of failure in time domain for reliability fatigue-based of a leaf spring in terms of random road strain loads.

Acknowledgement

The authors would like to express their gratitude to Universiti Kebangsaan Malaysia (Research funding: FRGS/1/2023/TK10/UKM/02/1 & GUP-2022-013) for supporting this research.

References

1. Zhang N, Jiang G, Wu D, Chen H, Wu J. Fatigue reliability analysis of the brake pads considering strength degradation. Eksploatacja i Niezawodność – Maintenance and Reliability 2020; 22(4): 620-626. https://doi.org/10.17531/ein.2020.4.5.
2. Li R, Yang Z, Chen G, Wu B. Analytical solutions for nonlinear deflections of corner-fillet leaf-springs. Mechanism and Machine Theory 2021; 157: 104182, https://doi.org/10.1016/j.mechmachtheory.2020.104182.
3. Hryciów Z, Krasoń W, Wysocki J. The experimental tests on the friction coefficient between the leaves of the multi-leaf spring considering a condition of the friction surfaces. Eksploatacja i Niezawodność – Maintenance and Reliability 2018; 20(4): 682-688. https://doi.org/10.17531/ein.2018.4.19.
4. Tran-Ngoc H, Khatir S, Le-Xuan T, Roeck G D, Bui-Tien T, Abdel-Wahab M. Finite element model updating of a multispan bridge with a hybrid metaheuristic search algorithm using experimental data from wireless triaxial sensors. Engineering with Computers 2022; 38(3): 1865–1883, https://doi.org/10.1007/s00366-021-01307-9.
5. Vu-Huu T, Le-Thanh C, Nguyen-Xuan H, Abdel-Wahab M. Polygonal Finite Element for Two-Dimensional Lid-Driven Cavity Flow. Computers, Materials & Continua 2022; 70(3): 4217–4239, https://doi.org/10.32604/cmc.2022.020889.
6. Ling Y, Ni J, Antonissen J, Hamouda H B, Voorde J V, Wahab M A. Numerical prediction of microstructure and hardness for low carbon steel wire Arc additive manufacturing components. Simulation Modelling Practice and Theory 2023; 122: 102664, https://doi.org/10.1016/j.simpat.2022.102664.
7. Nguyen K D, Thanh C -L, Vogel F, Nguyen-Xuan H, Abdel-Wahab M. Crack propagation in quasi-brittle materials by fourth-order phase-field cohesive zone model. Theoretical and Applied Fracture Mechanics 2022; 118: 103236, https://doi.org/10.1016/j.tafmec.2021.103236.
8. Tran V -T, Nguyen T -K, Nguyen-Xuan H, Abdel Wahab M. Vibration and buckling optimization of functionally graded porous microplates using BCMO-ANN algorithm. Thin-Walled Structures 2023; 182(Part B): 110267, https://doi.org/10.1016/j.tws.2022.110267.
9. Pastorcic D, Vukelic G, Bozic Z. Coil spring failure and fatigue analysis. Eng Fail Anal 2019; 99: 310-318, https://doi.org/10.1016/j.engfailanal.2019.02.017.
10. Giannakis E, Savaidis G. Local stress based fatigue assessment of multiaxially stressed automotive antiroll bars. Eng Fail Anal 2021; 126: 105472, https://doi.org/10.1016/j.engfailanal.2021.105472.
11. Thillikkani S, Nataraj M, King M F L. Failure analysis of Shackle Bracket in Airbus suspension under dynamic loading conditions. Eng Fail Anal 2021; 120: 105087, https://doi.org/10.1016/j.engfailanal.2. 020.105087.
12. Bakir M, Ozmen B, Donertas C. Correlation of Simulation, Test Bench and Rough Road Testing in terms of Strength and Fatigue Life of a Leaf Spring. Procedia Eng 2018; 213: 303-312, https://doi.org/10.1016/j.proeng.2018.02.031.
13. Li H -W -X, Chelidze D. Fatigue life estimation of structures under statistically and spectrally similar variable amplitude loading. Mech Syst Signal Proc 2021; 161: 107856, https://doi.org/10.1016/j.ymssp.2021.107856.
14. Zhang L, Jiang B, Zhang P, Yan H, Xu X, Liu R, Tang J, Ren C. Methods for fatigue-life estimation: A review of the current status and future trends. Nanotechnol. Precis. Eng. 2023; 6(2): 025001, https://doi.org/10.1063/10.0017255.
15. Abdullah L, Singh S S K, Abdullah S, Azman A. H, Ariffin A K, Kong Y S. The needs of power spectral density in fatigue life prediction of heavy vehicle leaf spring, Journal of Mechanical Science and Technology 2020; 34(6): 2341-2346, http://doi.org/10.1007/s12206-020-0510-z.
16. VanDerHorn E, Wang Z, Mahadevan S. Towards a digital twin approach for vessel-specific fatigue damage monitoring and prognosis.

Reliab Eng Syst Saf 2022; 219: 108222, https://doi.org/10.1016/j.ress.2021.108222.
17. Szmytka F, Charkaluk E, Constantinescu A, Osmond P. Probabilistic Low Cycle Fatigue criterion for nodular cast-irons. Int J Fatigue 2020; 139: 105701, https://doi.org/10.1016/j.ijfatigue.2020.105701.
18. Gong C, Frangopol D M. Time-variant hull girder reliability considering spatial dependence of corrosion growth, geometric and material properties. Reliab Eng Syst Saf 2020; 193: 106612, https://doi.org/10.1016/j.ress.2019.106612.
19. Long X Y, Liu K, Jiang C, Xiao Y, Wu S C. Uncertainty propagation method for probabilistic fatigue crack growth life prediction. Theoretical and Applied Fracture Mechanics 2019; 103: 102268, https://doi.org/10.1016/j.tafmec.2019.102268.
20. Fernández-Canteli A, Castillo E, Blasón S. A methodology for phenomenological analysis of cumulative damage processes. Application to fatigue and fracture phenomena. Int J Fatigue 2021; 150: 106311, https://doi.org/10.1016/j.ijfatigue.2021.106311.
21. Muth A, John R, Pilchak A, Kalidindi S R, McDowell D L. Analysis of Fatigue Indicator Parameters for Ti-6Al-4V microstructures using extreme value statistics in the HCF regime. Int J Fatigue 2021; 145: 106096, https://doi.org/10.1016/j.ijfatigue.2020.106096.
22. Mendler A, Döhler M, Ventura C E. A reliability-based approach to determine the minimum detectable damage for statistical damage detection. Mech Syst Signal Proc 2021; 154: 107561, https://doi.org/10.1016/j.ymssp.2020.107561.
23. Braga J A P, Andrade A R. Multivariate statistical aggregation and dimensionality reduction techniques to improve monitoring and maintenance in railways: The wheelset component. Reliab Eng Syst Saf 2021; 216: 107932, https://doi.org/10.1016/j.ress.2021.107932.
24. Zheng G, Liao Y, Chen B, Zhao S, Wei H. Multi-axial load spectrum extrapolation method for fatigue durability of special vehicles based on extreme value theory. Int J Fatigue 2024; 178; 108014, https://doi.org/10.1016/j.ijfatigue.2023.108014.
25. Wang J, You S, Wu Y, Zhang Y, Bin S. A Method of Selecting the Block Size of BMM for Estimating Extreme Loads in Engineering Vehicles. Mathematical Problems in Engineering 2016; 2016; 6372197, https://doi.org/10.1155/2016/6372197.
26. Putra T E, Husaini, Ikbal M, Automotive suspension component behaviors driven on flat and rough road surfaces, Heliyon 2021; 7(7): e07528, https://doi.org/10.1016/j.heliyon.2021.e07528.
27. Haiba M, Barton D C, Brooks P C, Levesley M C. The development of an optimisation algorithm based on fatigue life. Int J Fatigue 2003; 25(4): 299-310, https://doi.org/10.1016/S0142-1123(02)00143-3.
28. Konvicny D, Makys P, Furmanik M. Effect of increasing the sampling frequency with respect to the bandwidth of the PI controller of current control loop. Transportation Research Procedia 2021; 55: 935-940, https://doi.org/10.1016/j.trpro.2021.07.190.
29. Kong Y S, Abdullah S, Haris S M, Omar M Z, Schramm D. Generation of artificial road profile for automobile spring durability analysis. Jurnal Kejuruteraan 2018; 30(2): 123-128, http://dx.doi.org/10.17576/jkukm-2018-30(2).
30. Rashid A A A, Poi A, Jawi Z, Kassim K A. Revisiting Speed Management Strategies in Malaysia. Journal of the Society of Automotive Engineers Malaysia 2021; 5(2): 318–330, https://doi.org/10.56381/jsaem.v5i2.175.
31. Marques J M E, Benasciutti D. Variance of the fatigue damage in non-Gaussian stochastic processes with narrow-band power spectrum. Structural Safety 2021; 93: 102131, https://doi.org/10.1016/j.strusafe.2021.102131.
32. Kang J, Lu Y, Zhao B, Luo H, Meng J, Zhang Y. Remaining useful life prediction of cylinder liner based on nonlinear degradation model. Eksploatacja i Niezawodność – Maintenance and Reliability 2022; 24(1): 62-69, https://doi.org/10.17531/ein.2022.1.8.
33. Ren S, Chen H, Zheng R. Modified time domain randomization technique for multi-shaker non-stationary non-Gaussian random vibration control. Mech Syst Sig Proc 2024; 213: 111311, https://doi.org/10.1016/j.ymssp.2024.111311.
34. Sofi A, Giunta F, Muscolino G. Fatigue life bounds for randomly excited structures with interval parameters via sensitivity analysis. Prob Eng Mech 2022; 69: 103307, https://doi.org/10.1016/j.probengmech.2022.103307.
35. Fan W, Li Z, Yang X. A spectral method for fatigue analysis based on nonlinear damage model. Int J Fatigue 2024; 182: 108188, https://doi.org/10.1016/j.ijfatigue.2024.108188.
36. Mysior M, Pietrucha G, Koziołek S. Strength testing of a modular trailer with a sandwich platform. Eksploatacja i Niezawodność – Maintenance and Reliability 2022; 24(1): 163-169, https://doi.org/10.17531/ein.2022.1.18.
37. Pham Q H, Antoni J, Tahan A, Gagnon M, Monette C. Simulation of non-Gaussian stochastic processes with prescribed rainflow cycle count using short-time Fourier transform. Prob Eng Mech 2022; 68: 103220, https://doi.org/10.1016/j.probengmech.2022.103220.
38. Cazin D, Braut S, Božić Ž, Žigulić R. Low cycle fatigue life prediction of the demining tiller tool. Eng Fail Anal 2020; 111: 104457, https://doi.org/10.1016/j.engfailanal.2020.104457.

39. Zhu S -P, Lei Q, Huang H -Z, Yang Y -J, Peng W. Mean stress effect correction in strain energy-based fatigue life prediction of metals, Int J Damage Mech 2017; 26(8): 1219, https://doi.org/10.1177/1056789516651920.
40. El-Zeghayar M, Topper T, Bonnen J J. Derivation of Effective Strain-Life Data, Crack Closure Parameters and Effective Crack Growth Data from Smooth Specimen Fatigue Tests SAE Int J Mater Manf 2013; 6: 576–588, https://doi.org/10.4271/2013-01-1779.
41. Xia F -L, Zhu S -P, Liao D, Dantas R, Correia J A F O, De Jesus A M P. Isodamage curve-based fatigue damage accumulation model considering the exhaustion of static toughness. Eng Fail Anal 2020; 115: 104575, https://doi.org/10.1016/j.engfailanal.2020.104575.
42. Kadhim N A, Abdullah S, Ariffin A K. Effective strain damage model associated with finite element modelling and experimental validation. Int J Fatigue 2012; 36: 194–205, https://doi.org/10.1016/j.ijfatigue.2011.07.012.
43. Nagode M, Oman S, Klemenc J, Panić B. Gumbel mixture modelling for multiple failure data. Reliab Eng Syst Saf 2023; 230: 108946, https://doi.org/10.1016/j.ress.2022.108946.
44. Xiang G, Bacharoudis K C, Vassilopoulos A P. Probabilistic fatigue model for composites based on the statistical characteristics of the cycles to failure. Int J Fatigue 2022; 163; 107085, https://doi.org/10.1016/j.ijfatigue.2022.107085.
45. Pourdavood M, Bocher P. Statistical modeling of microstructurally short crack growth in high cycle fatigue. Materials Science & Engineering A 2024; 146092, doi: https:// doi.org/10.1016/j.msea.2024.146092.
46. Wang Y, Xia A, Qin G. Probabilistic modeling for reliability analysis of buried pipelines subjected to spatiotemporal earthquakes. Prob Eng Mech 2022; 69: 103315, https://doi.org/10.1016/j.probengmech.2022.103315.
47. Selech J, Andrzejczak K. An aggregate criterion for selecting a distribution for times to failure of components of rail vehicles. Eksploatacja i Niezawodność – Maintenance and Reliability 2020; 22(1): 102-111. https://doi.org/10.17531/ein.2020.1.12.
48. Li X, Li S, Li J, Su Y. Nonstationary time-varying extreme value of downburst-induced wind loads based on transformed stationary method. Prob Eng Mech 2022; 70: 103345, https://doi.org/10.1016/j.probengmech.2022.103345.
49. Wang C, Liu Y, Wang D, Wang G, Wang D, Yu C. Reliability evaluation method based on dynamic fault diagnosis results: A case study of a seabed mud lifting system. Reliab Eng Syst Saf 2021; 214: 107763, https://doi.org/10.1016/j.ress.2021.107763.
50. Venturini S, Rosso C, Velardocchia M. An automotive steel wheel digital twin for failure identification under accelerated fatigue tests. Eng Fail Anal 2024; 158: 107979, https://doi.org/10.1016/j.engfailanal.2024.107979.
51. Żyluk A, Zieja M, Grzesik N, Tomaszewska J, Kozłowski G, Jasztal M. Implementation of the Mean Time to Failure Indicator in the Control of the Logistical Support of the Operation Process. Appl Sci 2023; 13(7): 4608, https://doi.org/10.3390/app13074608.
52. Schumacher J, Clausen B. Calculation of the Fatigue Limit of High-Strength Steel Specimens at Different Loading Conditions Based on Inclusion Sizes. Steel Research Int 2021; 92: 2100252, https://doi.org/10.1002/srin.202100252.
53. Li H, Deng Z -M, Golilarz N A, Soares C G. Reliability analysis of the main drive system of a CNC machine tool including early failures. Reliab Eng Syst Saf 2021; 215: 107846, https://doi.org/10.1016/j.ress.2021.107846.